Three-Dimensional Imaging of Microstructure in Au Nanocrystals

G. J. Williams, M. A. Pfeifer, I. A. Vartanyants,* and I. K. Robinson
Department of Physics, University of Illinois, Urbana, Illinois 61801
(Received 19 November 2002; published 29 April 2003)

X-ray diffraction using a coherent beam involves the mutual interference among all the extremities of small crystals. The continuous diffraction pattern so produced can be phased because it can be oversampled. We have thus obtained three-dimensional images of the interiors of Au nanocrystals that show 50 nm wide bands of contrast with {111} orientation that probably arise from internal twinning by dynamic recrystallization during their formation at high temperature.

DOI: 10.1103/PhysRevLett.90.175501 PACS numbers: 61.10.Nz, 42.30.Rx, 61.46.+w, 68.37.Yz

Deformation of metals is understood to involve complex concerted motions of the dislocations that inevitably break the perfection of their individual crystalline grains, which are usually nanometers to microns in size [1]. Electron microscopy (EM) is the most widely used technique for dissecting this internal microstructure. The relatively strong interaction of electrons with condensed matter means that the method is limited to viewing either the exterior surfaces of microstructures [scanning EM (SEM)] or else 2D projections through thin slices [transmission EM], which requires destructive sample preparations. It is highly desirable to find a nondestructive way of imaging the interiors of material grains in 3D so that arbitrary views can be investigated. This is analogous to the advances in medicine that followed the development of computed tomography methods in the 1970s [2,3]. Microtomographic methods for 3D imaging of materials have since been developed [4,5]. The advantage of sections over projection views is that microstructural features are unambiguously localized in 3D.

Coherent x-ray diffraction (CXD) is a rapidly developing technique [6] that opens opportunities for the study of both dynamics of condensed-matter systems and their structure. The method has become available by the recent development of high-brilliance third-generation sources of synchrotron radiation, such as the Advanced Photon Source (APS). In favorable circumstances, the beam's coherence volume, which is directly proportional to the source brilliance, can entirely enclose a small crystal. Diffraction from all parts of the crystal then undergoes wave superposition which leads to a highly structured CXD pattern. If high-quality x-ray lenses were available, as they are for electrons, such diffraction patterns could be transformed to magnified images directly. In spite of widespread efforts to develop such x-ray microscopes [7,8], they are still not competitive with EM.

In this Letter, we show that the objective lens of an x-ray microscope can be replaced by a computation that inverts a 3D measurement of the amplitude of a CXD pattern to a 3D image. The computation relies on the fact that the diffraction can be *oversampled* relative to its spatial Nyquist frequency, so that the Fourier transform can be overdetermined in spite of the missing phase information. We apply the method to the 3D imaging of nanocrystals of Au obtained by high-temperature coalescence from an evaporated polycrystalline thin film. We find residual internal texture that could be attributed to twinning which might originate from dynamic recrystallization of defects introduced during their formation.

When a crystal is illuminated by a coherent x-ray beam, the intensity distribution in the vicinity of a Bragg point forms a well-defined pattern. In the kinematical limit, this 3D CXD pattern is of the form of the square of a structure factor multiplied by a function:

$$I(\mathbf{q}) \propto \left| \int_0^\infty \rho_L(\mathbf{r}) s(\mathbf{r}) e^{i\mathbf{q}\cdot\mathbf{r}} e^{i\mathbf{q}\cdot\mathbf{u}(\mathbf{r})} d\mathbf{r} \right|^2. \quad (1)$$

The total electron density of the crystal is written as the product of the crystal lattice, $\rho_L(\mathbf{r})$, and a function describing the shape of the crystal, $s(\mathbf{r})$. Thus, the intensity distribution in reciprocal space is the convolution of the Fourier transform of the crystal shape with the reciprocal lattice of the bulk crystal. The function $\mathbf{u}(\mathbf{r})$ represents the strain field due to the displacement of atoms from their bulk structure sites; therefore strain inside the crystal gives rise to noncentrosymmetry in the CXD pattern. In an earlier paper we reported the inversion of a CXD pattern in 2D to arrive at the projection of a crystal onto a plane [9]. More recently, a 3D calculation of this kind has been achieved by Miao *et al.* [10]. Here we present the extension of our procedure, allowing the recovery of the 3D density distribution within the nanocrystal.

Since the intensity distribution in reciprocal space is a continuous one, the pattern around a Bragg peak can be sampled with arbitrary q spacing. This property allows the oversampling of such a pattern, leading to the collection of sufficient information to iteratively reconstruct the phase of the collected diffraction data. In 1982, Bates showed that nonunique solutions to such problems are pathologically rare in dimensions higher than one [11]. While noise in the data increases the probability of

ambiguous solutions, it is possible to regain a unique solution by applying an appropriate constraint [12].

To understand the oversampling requirement in 1D, we write the amplitude of the intensity collected in pixel m in a detector of N pixels as the discrete Fourier transform:

$$F(m\Delta q_x) = \sum_{n=1}^{N} \rho(n\Delta x) e^{i2\pi mn/N}, \qquad (2)$$

where Δq_x is the size of a pixel in the detector, Δx is the real space sampling, related by $\Delta x = 2\pi/N\Delta q_x$. It is clear from (2) that F is a periodic function with N distinct values of m. In real space, we define a support region, N', that encompasses the entirety of the diffracting density, i.e., $\rho(n\Delta x) = 0$, for all n such that $N' < n \leq N$. Then, the oversampling ratio, σ, is simply the ratio of the size of the entire array to the size of the support, $\sigma = N/N'$. In reciprocal space, the oversampling ratio is given by the ratio of the number of points measured per oscillation of the transform (2) to the number of points necessary to define an oscillation, which is the Nyquist sampling rate. These oscillations are readily seen as fringes in the experimental data. Even if we assume the real space density, $\rho(x)$, is purely real, we have N unknowns and only $N/2$ measurements, because $F(q_x) = F^*(-q_x)$. Therefore, σ must be at least 2 in order for it to be possible to invert (2), i.e., to phase the diffraction pattern. The extension from 1D to 3D is trivial because the equation counting argument is the same. We introduce a separate measure of oversampling for each dimension, $\sigma = \sigma_x\sigma_y\sigma_z$, with $\sigma \geq 2$. Millane has shown, using simulations, that in the case with two of the σ_i's greater than 2, the requirement on the oversampling in the third dimension is relaxed to sampling at the Nyquist frequency, $\sigma_j = 1$ [13].

The phasing of an oversampled diffraction pattern may be accomplished through the use of an iterative method [14], utilizing known information to find a set of phases consistent with the measured data. Such methods have been used successfully in similar situations, for example, electron scattering measurements [14] and transmission x-ray studies of nonperiodic materials [15]. The fitting begins by assigning a set of random phases to the support and evaluating (2) using a fast Fourier transform, which yields a first "guess" at the diffraction pattern in reciprocal space. The amplitude of the guess is then overwritten with the measured amplitude and back transformed to yield a complex density in real space. After applying an appropriate real space constraint—for example, enforcing a finite support and converting the density to a real, non-negative function—it is transformed back to reciprocal space. This cycle is repeated until the search converges to a solution.

The method described above is called the error reduction (ER) method [16]. The ER method may be modified to propagate the result of previous iterations, giving various "input/output methods" [16]. The hybrid input/output (HIO) method of Millane incorporates a parameter, β, defining a fraction of the previous cycle's result to combine with the current result. Additionally, the real space constraint is relaxed by allowing a small amount of amplitude, ϵ, to exist outside the support [17].

In order to conduct a CXD experiment, the spatial extent of the diffracting density must be smaller than the coherence volume of the incident beam. The insertion device at Sector 33 of the APS, with a source size of $\sigma_x = 240\ \mu$m and $\sigma_y = 16\ \mu$m, gives transverse coherence lengths greater than 5 μm. The longitudinal coherence is determined to be 6 μm by a Si(333) monochromator at 9.5 keV.

Diffraction patterns were collected with a direct-reading CCD, whose pixel size is 22.5 μm $\times$ 22.5 μm, located 2.8 m from the sample. A 2D CXD pattern was collected near a {111} Bragg peak for 5–10 min. In order to collect a full 3D pattern we rotated the sample through the Bragg condition in steps of 0.002° acquiring a sequence of nearly parallel 2D slices, as shown in Fig. 1, which were then stacked to obtain a sampled 3D pattern. This procedure is equivalent to shifting the detector perpendicular to the Ewald sphere in reciprocal space. Because the 3D diffraction pattern surrounds a reciprocal lattice point located far from the origin, the entire measurement spans an angular range of only 0.1°. By contrast, the forward-scattering version of the experiment [10] requires a 180° range.

To form crystals smaller than the coherence volume, a 100 nm Au film was deposited onto a Si(100) wafer, with the native oxide intact, at room temperature forming a conventional {111} textured polycrystalline film. The sample was then placed in a radiative heating cell, which was mounted on the goniometer, capable of achieving temperatures up to the melting point of Au. Temperature was measured by a thermocouple affixed to the back of the sample and by tracking the expansion of the lattice and comparing with tabulated values [18].

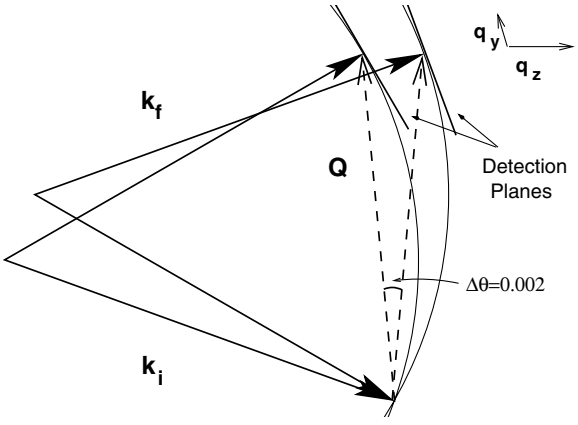

FIG. 1. Experimental geometry. As the sample is rocked, 2D slices are collected through the 3D CXD pattern.

As the film was heated to near its melting point, it spontaneously dewetted from the Si/SiO_2 substrate in less than 20 h at 1000 °C. The film first formed one-dimensional "rivers," before splitting at grain boundaries into small single crystalline islands. This procedure resulted in shapes similar to the well-known equilibrium shapes [19] with a distribution of sizes in the micron range. SEM recorded this evolution after the preparation. Since an array of nanocrystals with different azimuthal orientations is illuminated by the x-ray beam, one nanocrystal can be selected and measured as a 3D rocking series. Three such slices acquired at 950 °C are shown in Fig. 2.

Certain information about the diffracting crystal may be discerned from the CXD pattern directly. The flares in reciprocal space correspond to facets of the crystal and the modulation of these flares to the spacing of parallel facets. Therefore, it is possible to make some conclusions about the size and general shape of the particle before the CXD pattern is phased. The size of the particle in a given direction is $2\pi/\Delta q_{\text{fringe}}$; hence the particle we measured is approximately 1 μm by 3 μm.

In the experimental geometry, we define our local reciprocal space axes as follows: $\mathbf{q}_x$ and $\mathbf{q}_y$ are mutually perpendicular and coplanar with the surface of the CCD, and $\mathbf{q}_z$ is perpendicular to $\mathbf{Q}$, the total scattering vector, as shown in Fig. 1. Thus, $\Delta q_x = \Delta q_y = 3.9 \times 10^{-4}$ nm^{-1} is the reciprocal space spanned by a pixel in the CCD.

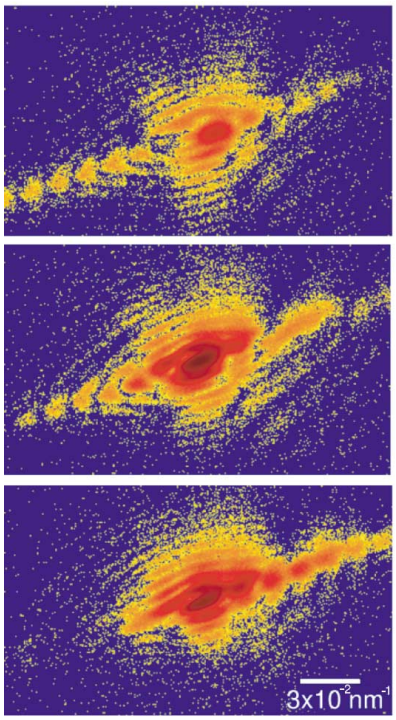

FIG. 2 (color online). Typical slices through the 3D CXD pattern of a Au crystal near the $(11\bar{1})$ reflection with spacing 2.8×10^{-3} nm^{-1}.

Rocking the sample gives a spacing of $\Delta q_z = 9.3 \times 10^{-4}$ nm^{-1} in the third direction. From Fig. 2 we can readily estimate the oversampling of the measurement. The data have a minimum of 15 pixels per fringe, so we may be confident that $\sigma_x \gg 2$ and $\sigma_y \gg 2$. The oversampling in the third direction, σ_z, can be estimated from the 2D fringe spacing, of order 5×10^{-3} nm^{-1}, and the step size, Δq_z. Thus, we expect that $\sigma_z > 2$, satisfying the oversampling condition.

Once the 2D slices have been collected, they are stacked to form a 3D reciprocal space constraint used during the fitting. We define an error metric in reciprocal space: $\chi^2 = \sum_{i=1}^{N} (F_i^C - \sqrt{I_i^M})^2 / \sum_{i=1}^{N} I_i^M$ where F_i^C is the amplitude at pixel i in the current fit, $\sqrt{I_i^M}$ is the amplitude of pixel i in the measured CXD pattern, and N is the total number of pixels in the $440 \times 440 \times 30$ array used. Each fit consists of 2300 iterations, alternating between the ER and HIO algorithms, with a real space constraint box of dimension $100 \times 100 \times 20$ pixels. Since the ER is prone to stagnation near local minima of the error metric [12], we performed 50–100 cycles of HIO after each 150–250 cycles of ER. In our calculations, the best results were obtained with the values $\epsilon = 0.01$ and β between 0.75 and 0.85 in the HIO algorithm.

The resolution—the period of the finest feature detectable—of the real space reconstruction is $\Delta\Gamma = 2\pi/\Delta q_{\text{max}}$, where Δq_{max} is the radius in q space beyond which the diffracted intensity had dropped to the noise level. This resolution might be improved by extending the exposure time. For the data shown in Fig. 2, we estimate our resolution to be $\Delta\Gamma_{x,y} = 80$ nm and $\Delta\Gamma_z = 450$ nm. The 3D real space density corresponding to the reconstructed phase and measured amplitude of the CXD pattern is shown in Fig. 3. The reciprocal space fits have $\chi^2 = 0.04$, which corresponds to an uncertainty of about 20% per pixel. The two best real space reconstructions obtained from 15 sets of random starting phases are shown in Fig. 3. Using a measure of real space reproducibility analogous to χ^2, i.e., by comparing the fit amplitudes, we find the disagreement to be 0.033. This quantity is 3×10^{-5} for the corresponding reciprocal space reconstructions. We interpret this reproducibility to be a measure of the experimental uniqueness, since true uniqueness is not assured with noisy data [12].

As expected, the 3D CXD real space images have higher contrast than the 2D projections reported previously [9]. The diamond shaped region of high intensity is believed to be an artifact caused by the partial coherence of the incident beam [20]—specifically, a Be window 6 m from the sample. The crystal's external morphology is an elongated-disk with well-developed [111] facets on the top and bottom surfaces, parallel to the substrate. This [111] plane appears diagonally in the side-view sections shown because of the coordinate transformation of the diffractometer operating in a grazing-exit geometry [21]. The faces are clearly visible, but it is not possible to

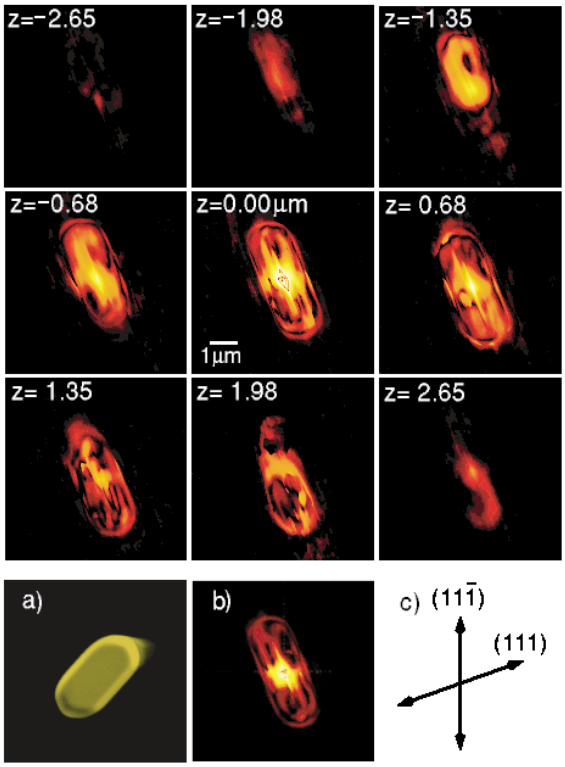

FIG. 3 (color online). Top: The 2D slices through the best fit 3D reconstructed density separated as labeled. Bottom: (a) SEM image of a Au nanocrystal prepared as described in the text. (b) $z = 0.00$ μm slice from the second best fit showing good agreement between fits. (c) Coordinate system for the reconstructed crystal.

distinguish between the top and bottom sides of the image. The density appears above center in the early sections ($z \simeq -1.35$ μm) and below center in the later sections ($z \simeq 1.35$ μm), consistent with an oval morphology sectioned obliquely. The (11$\bar{1}$) reflection, which was used for imaging, points directly up the page [21]. This can be seen to lie at the correct 70.5° angle to the (111) direction.

The internal density contrast is in the form of bright and dark bands oriented parallel to both the [111] and [11$\bar{1}$] directions in the images. The [111] bands have a width of 50 nm, a period of 100 nm, and a lateral extent of 600 nm, both within the section and between adjacent sections. The [11$\bar{1}$] bands have the same width and are slightly less extended. Although dynamical scattering and series termination effects may play a role in the appearance of these features, we interpret these to be deformation bands associated with the sample preparation. The dark region of the band presumably corresponds to material with twinned stacking that would diffract in a direction different from the (11$\bar{1}$) imaging direction. Such bands are known to occur in soft fcc metals and are attributed to recrystallization following slippage along [111] planes during deformation [22]. Given the oval, elongated-disk morphology of our nanocrystal samples, it is clear that they have not yet reached an equilibrium shape in their growth out of the polycrystalline starting film. It is therefore not surprising that residual deformation defects are observed.

In conclusion, we have obtained 3D images of microstructure by inversion of a coherent diffraction pattern. Our method differs from related experiments [10] in that the entire pattern may be measured directly. Because Bragg diffraction is involved, all artifacts due to air or slit scatter and other grains are avoided and a strong sensitivity to strain results.

We are grateful to C. Benson for technical assistance. This research was supported by the NSF under Grant No. DMR98-76610. The UNICAT facility at the APS is supported by the University of Illinois, Materials Research Laboratory (DOE Contract No. DEFG02-91ER45439, the State of Illinois-IBHE-HECA, and the NSF), the ORNL, NIST, and UOP LLC. The APS is supported by the DOE under Contract No. W-31-109-ENG-38. SEM work was carried out in the Center for Microanalysis of Materials, University of Illinois.

*On leave from Institute of Crystallography RAS, Leninsky pr. 59, 11733 Moscow, Russia.

[1] A. H. Cottrell, *The Mechanical Properties of Metals* (Wiley, New York, 1964).
[2] P. Wells, J. Davis, and M. Morgan, Mater. Forum **18**, 111 (1994).
[3] A. C. Kak and M. Slaney, *Principles of Computerized Tomographic Imaging* (SIAM, Philadelphia, PA, 2001).
[4] P. Cloetens *et al.*, Europhys. News **32**, 46 (2001).
[5] Y. Wang *et al.*, Rev. Sci. Instrum. **72**, 2062 (2001).
[6] M. Sutton *et al.*, Nature (London) **352**, 608 (1991).
[7] C. Jacobsen and J. Kirz, Nat. Struct. Biol. **5**, 650 (1998).
[8] W. Meyer-Ilse *et al.*, Synchrotron Radiation News **8**, 29 (1993).
[9] I. K. Robinson, *et al.*, Phys. Rev. Lett. **87**, 195505 (2001).
[10] J. Miao *et al.*, Phys. Rev. Lett. **89**, 088303 (2002).
[11] R. H. T. Bates, Optik **61**, 247 (1982).
[12] J. H. Seldin and J. R. Fienup, J. Opt. Soc. Am. A **7**, 412 (1990).
[13] R. P. Millane, J. Opt. Soc. Am. A **13**, 725 (1996).
[14] R. W. Gerchberg and W. O. Saxton, Optik **35**, 237 (1972).
[15] J. Miao, P. Charalambous, J. Kirz, and D. Sayre, Nature (London) **400**, 342 (1999).
[16] J. R. Fienup, Appl. Opt. **21**, 2758 (1982).
[17] R. P. Millane and W. J. Stroud, J. Opt. Soc. Am. A **14**, 568 (1997).
[18] Y. S. Touloukian, *Thermophysical Properties of Matter Vol. 12* (IFI/Plenum, New York, 1975).
[19] J. C. Heyraud and J. J. Metois, Acta Metall. **28**, 1789 (1980).
[20] I. A. Vartanyants and I. K. Robinson, J. Phys. Condens. Matter **13**, 10593 (2001).
[21] J. A. Pitney *et al.*, Phys. Rev. B **62**, 13 084 (2000).
[22] H. W. Hayden, W. G. Moffat, and J. Wulff, *Structure and Properties of Materials III* (Wiley, New York, 1965).